Journal of Materials Chemistry B

RSC Publishing

PAPER

View Article Online
View Journal | View Issue

Cite this: *J. Mater. Chem. B*, 2013, **1**, 2851

DNA-responsive disassembly of AuNP aggregates: influence of nonbase-paired regions and colorimetric DNA detection by exonuclease III aided amplification†

Zhixin Zhou, Wei Wei, Yuanjian Zhang* and Songqin Liu*

Received 12th February 2013
Accepted 10th April 2013

DOI: 10.1039/c3tb20206b

www.rsc.org/MaterialsB

Due to great potential in nanobiotechnology, nanomachines, and smart materials, DNA-directed disassembly of gold nanoparticles (AuNPs) has been extensively explored. In a typical system, nonbase-paired regions (*e.g.*, overhangs and gaps in the linker DNA and oligonucleotide spacers between thiol group and hybridization sequence) are indispensable portions in the disassembly of AuNPs based on DNA displacement reaction. Therefore, it is necessary to study the effect of nonbase-paired regions to improve the kinetics of disassembly of AuNPs. Herein, the disassembly rate of AuNPs based on DNA displacement reaction was investigated by using different length spacers and linker DNA containing various lengths of gaps or overhangs. Interestingly, it was revealed that among the gaps in the linker DNA could be most effectively used to improve the disassembly rate of the AuNPs. As a result, when we introduced gaps into linker DNA, the DNA displacement reaction of AuNPs was markedly shortened to less than 50 min, which was much faster than the previous methods. As a proof of the importance of our findings, a rapid AuNP-based colorimetric DNA biosensor has been successfully prepared. In addition, we showed that the signal of the biosensors could be further amplified using exonuclease III, resulting in a much lower detection limit in comparison with previous sensors similarly using AuNP aggregates as probes.

Introduction

Due to its high stability, tremendous recognition properties, and predictable secondary structure, DNA has been widely applied to the assembly of nanomaterials in the past few years.[1–4] It is attractive that the assembly process could be precisely controlled by tailoring the length of DNA, regulating the DNA structure and sequence, and selecting suitable nanomaterials. Among them, DNA-directed assembly of gold nanoparticles (AuNPs) has attracted much attention because of its powerful programmable capability of DNA and distinguished assembly performance of AuNPs, thus it was widely used in the fields of smart materials,[5–7] nanomachines,[8] and biosensors.[9,10] For example, Mirkin and co-workers developed a three-component sandwich colorimetric biosensor containing linker DNA and two sets of DNA-modified AuNPs.[11,12] When the linker DNA (complementary with two sets of DNA-modified AuNPs) assembled AuNPs, the consequent aggregation of AuNPs triggered a color change. Analogous three-component sandwich structures have been widely adopted as colorimetric biosensors for various applications in terms of detection of DNA,[13] proteins,[14–16] metal ions,[17–19] and even small molecules.[20,21]

Recently, the reverse process taking advantages of target analytes to disassemble AuNP aggregates has also been proven to be one elegant platform for developing colorimetric biosensors. The redispersion of the AuNP aggregates accompanies a distinct color change, therefore, the reversible aggregations of DNA-modified AuNPs could also be used as colorimetric biosensors in principle. To control disassembly of DNA-linked AuNPs, physical, chemical and biological stimuli have been well studied, such as temperature,[22,23] enzymes,[24,25] proteins,[26] metal ions[27–29] and small molecules.[30,31] Compared with these disassembly methods, the DNA displacement reaction, firstly demonstrated by Niemeyer and co-workers,[32] shows some unique advantages.[33–35] For example, it is a highly selective way to disassemble AuNPs without the limitation of a specific-DNA sequence, thus providing a general facile way to fabricate nanomachines and biosensors. Despite their success in disassembly of materials using the DNA displacement reaction, the slow disassembly rate (up to 24 h) has not been well addressed yet.[32,36] Such a time-consuming process is not conducive to practical applications based on disassembly of AuNPs. Therefore, speeding up the DNA displacement reaction of AuNPs is an urgent challenge to be solved.

State Key Laboratory of Bioelectronics, School of Chemistry and Chemical Engineering, Southeast University, Nanjing, 211189, P.R. China. E-mail: liusq@seu.edu.cn; yuanjian.zhang@seu.edu.cn; Fax: +86-25-52090618; Tel: +86-25-52090613

† Electronic supplementary information (ESI) available: DNA sequence used in this study (Table S1), optimization of the linker DNA concentration and length (Fig. S1–S3) and more detailed discussions. See DOI: 10.1039/c3tb20206b

Previous studies demonstrated that nonbase-paired regions (*e.g.*, overhangs and gaps in the linker DNA and oligonucleotide spacers between thiol group and hybridization sequence, see scheme in Fig. 1) are indispensable portions in the disassembly of AuNPs based on the DNA displacement reaction. Overhangs in linker DNA could form more complementary paired bases to promote DNA displacement reaction.[6,8,32] For example, Sleiman and Aldaye applied overhang sequences to control the geometry of the discrete AuNP assemblies.[7] Gaps were recently introduced in the linker DNA to reversibly control the internanoparticle distance.[37] This was because internanoparticle distance was closely correlated to both *van der Waals* and electrostatic forces between AuNPs, which in turn significantly affected the duplex DNA stability and assembly–disassembly properties. For the same reason, oligonucleotide spacers were used to increase interparticle distance to improve the crowded environment of the DNA-cross-linked AuNP aggregates.[26,30,38] Given the importance of these nonbase-paired regions in the DNA-responsive disassembly of AuNPs, it is necessary to study their effect on the disassembly processes of AuNPs. However, other than the investigation of the effect of nonbase-paired regions on the T_m (melting temperature) of AuNP aggregates,[22,38,39] fundamental studies about the effect of nonbase-paired regions on the disassembly rate of AuNPs are few.

Herein, we reported a study on the disassembly rate of AuNPs using different length of gaps or overhangs in the linker DNA and oligonucleotide spacers between thiol group and hybridization sequence. Interestingly, it was found that among them the disassembly rate of AuNPs was mostly dominated by gaps in the linker DNA. For instance, when we introduced gaps into the linker DNA, the DNA displacement reaction based on AuNPs was markedly shortened to less than 50 min (nearly 30 times faster than that by conventional methods). As a proof of the importance of our findings, a rapid colorimetric biosensor was developed for detection of target DNA. In addition, exonuclease III was applied to AuNP-based colorimetric biosensors for further boosting the sensitivity of the DNA detection. Exonuclease III catalyzes the stepwise removal of mononucleotides from blunt or recessed 3′-hydroxyl termini of duplex DNAs.[40–44] Compared with other nucleases such as nicking endonuclease[45,46] and DNAenzyme,[47] exonuclease III does not require a specific recognition site, which may offer a universally adaptable system. Consequently, the detection limit of the proposed sensor could be reduced to 2 nM while those similarly using AuNP aggregates as probes in previous reports ranged from 20 nM to 50 μM.[26–31]

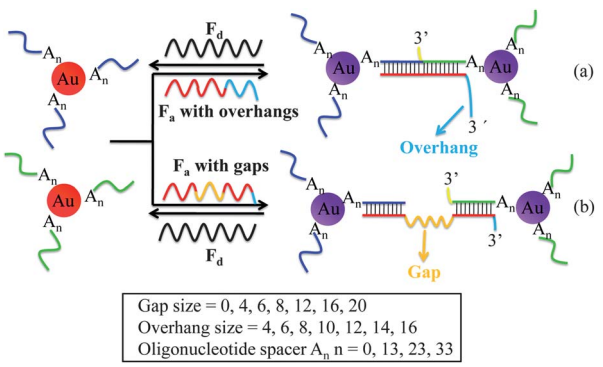

Fig. 1 Scheme of DNA-directed assembly and disassembly of DNA-functionalized AuNPs. Oligomer F_a contains overhangs (a) and gaps (b).

Experimental

1 Reagents

Exonuclease III was purchased from TAKARA biotechnology Co., Ltd. (Dalian China) and used without further purification. All oligonucleotides were obtained from Shanghai Sangon biotechnology Co., Ltd. (Shanghai China) and used as received. The sequence of synthesized oligonucleotides is given in Table S1 (ESI).† Trisodium citrate, $HAuCl_4$, NaH_2PO_4, Na_2HPO_4, and NaCl were of analytical grade and purchased from Sinopharm Chemical Reagent Co., Ltd. (Shanghai, China). Tween-20 was obtained from Sunshine biotechnology (Nanjing China) Co., Ltd. Tris(2-carboxyethyl)phosphine hydrochloride (TCEP) was provided by Thermo Scientific (USA). Double distilled water was used for all of the experiments.

2 Preparation of citrate-capped AuNPs

AuNPs were prepared by reducing $HAuCl_4$ with trisodium citrate according to previous reports.[48,49] Briefly, 5 mL of 38.8 mM trisodium citrate was added rapidly into a stirred boiling aqueous solution containing 50 ml of 1 mM $HAuCl_4$. The solution turned clear, black, purple and deep red in sequence within 2 min. After the solution was kept boiling and stirred for 15 min, it was naturally cooled to room temperature. The final colloidal solution was stored at 4 °C for further use. The concentration of AuNPs was 13 nM calculated using the Lambert–Beer law. The extinction coefficient of 2.7×10^8 M^{-1} cm^{-1} at 520 nm for 13 nm AuNPs was used in this work.[48]

3 Preparation of DNA-functionalized AuNPs

DNA-functionalized AuNPs were synthesized according to previous reports with minor modifications.[50–52] To activate the thiol–DNA, 20 μL of 100 μM DNA was added to 5 μL of 20 mM Tris buffer (pH 7.3) containing 100 mM TCEP. The resultant solution was incubated for 1 h at room temperature. After incubation, the activated oligonucleotides were purified using Millipore's Amicon Ultra-0.5 centrifugal filter device to remove excess TCEP. The freshly deprotected and purified DNA was later added to 500 μL of gold colloidal solution to functionalize the AuNPs. The mixed solution was sonicated for 10 s, and then incubated for 20 min with shaking at room temperature. After that, the resultant solution was mixed with 0.1 M phosphate buffer (pH 7.2) containing 0.1% sodium dodecyl sulfate (SDS) and the final concentrations of phosphate and SDS were brought to 0.01 M and 0.01%, respectively. The solution was sonicated for 10 s, and incubated for 20 min. In the subsequent salt aging process, the concentration of NaCl was first increased to 0.05 M using 2 M NaCl. The process was repeated with one more increment of 0.05 M NaCl and for every 0.1 M NaCl increment thereafter until a concentration of 0.5 M NaCl was

reached. After each addition of NaCl, the DNA–AuNPs were vortexed, sonicated for 10 s, and then incubated for 20 min. After the salt aging, the mixture was shaken at room temperature overnight. To remove excess DNA, the solution was centrifuged at 13 200 rpm for 20 min, and then redispersed in reaction buffer (pH 8.0) containing 20 mM Tris, 200 mM NaCl, 5 mM $MgCl_2$, and 0.05% Tween-20. Tween-20 was used to reduce the sticking of AuNPs to the Eppendorf tube in this work.[50] This step was repeated three times to sufficiently remove excess DNA. The good stability in the salt aging process confirmed the successful coupling of DNA to AuNPs (see Fig. S1†).

4 Formation of DNA-cross-linked AuNP aggregates

In practical applications, both a high degree of aggregation and rapid rate of DNA-responsive disassembly of AuNPs are desired, thus the concentration of linker DNA was optimized as 100 nM in this study (see Fig. S2 and more discussion in ESI†). Typically, thiol–DNA1 and DNA2-modified AuNPs were mixed. 1 μL of 100 μM linker DNA was added to the mixed AuNP solution so that the concentration of linker DNA was 100 nM. The mixture was heated to 70 °C and incubated for 5 min. After that, the solution was cooled to room temperature, during which the color of the solution changed from red to purple, and finally a large amount of aggregates precipitated at the bottom of the centrifuge tube. To ensure homogeneity and reproducibility of AuNP aggregates, all solutions were vigorously agitated before use.

5 Kinetic disassembly investigation

2 μL of the complementary target, which was used to give the final concentration of 200 nM, was added to a solution (100 μL) of the as-prepared DNA-cross-linked AuNP aggregates to initiate the disassembly of AuNPs. The mixed solution was incubated for 2 h at 37 °C, and the absorption spectra were monitored using a UV-visible spectrometer.

6 Colorimetric assay of oligonucleotides based on exonuclease III assisted signal amplification

A 1 μL aliquot of sample solution containing varying concentrations of target was added to 99 μL of solution of as-prepared DNA-cross-linked AuNP aggregates. Then, 60 U exonuclease III was added to the mixed solution followed by incubation at 37 °C for 2 h. After that, the solutions were monitored by UV-visible spectra or directly observed using the "naked" eye.

7 Characterization

UV-vis spectra were taken using a UV-visible spectrometer (Shimadzu UV-2450, Kyoto, Japan). Transmission electron microscopy (TEM, JEM-2010, Hitachi, Japan) was used to characterize the morphologies of mono-dispersed AuNPs and AuNP aggregates before and after digestion by adding exonuclease III and target. The sample was prepared by dropping 10 μL of sample solution onto a carbon-coated copper grid and drying at room temperature.

Results and discussion

1 The effect of nonbase-paired regions on disassembly kinetic of AuNPs

1.1 Assay formats. To evaluate the disassembly rate, two sets of DNA-functionalized AuNPs were designed. One was functionalized with 5′-thiol-modified DNA (DNA1) which had a 12-mer sequence for hybridization (Fig. 1, colored in green), 5 protruding nucleotides (colored in yellow) at the 3′ termini of DNA1 to prevent the exonuclease III from digesting the DNA1 in next DNA detection experiment, and various numbers of oligonucleotide spacers (A_n n = 0, 13, 23, 33). The other was functionalized with 3′-thiol-modified DNA that had a 12-mer sequence for hybridization and a 10-nucleotide spacer (DNA2, Fig. 1, colored in blue). Two complementary fueling oligonucleotides, F_a and F_d (Fig. 1), were used to assemble or disassemble AuNPs, respectively. Various numbers of overhangs (Fig. 1a, colored in light blue) and gaps (Fig. 1b, colored in orange) were present in oligomer F_a. Upon addition of oligomer F_a to the mixture of DNA1–AuNPs and DNA2–AuNPs, the color of the mixed AuNPs solution changed from red to purple, and finally AuNP aggregates were precipitated at the bottom of tube, resulting in a colorless supernatant. In the disassembly step, to restore the original absorption of dispersed AuNPs solution, two equivalents of oligomer F_d (with respect to F_a, 200 nM) was added in the AuNP aggregates solution.[32] Oligomer F_d was complementary with and hybridized with oligomer F_a to form a more stable double helical structure *via* nonbase-paired regions (gaps or overhangs), resulting in disassembly of AuNP aggregates. Upon disassembly, the color of the supernatant of AuNP aggregates solution turned from colorless to red gradually, allowing convenient monitoring of disassembly rate. To quick screen which is the rate-limited nonbase-paired region, we fixed the disassembly time (*e.g.* 2 h) for each region. This methodology was previously used to study the assembly process of AuNPs.[39]

1.2 Effect of overhang in oligomer F_a on the disassembly rate of AuNPs. To study the effect of overhangs, DNA2 with a 10-nucleotide spacer and DNA1 with a 23-nucleotide spacer were used. Various lengths of overhangs were introduced at 3′ termini of oligomer F_a (see scheme in Fig. 1a). The absorbance ratio of 525 nm over 650 nm (A_{525}/A_{650}) was used to quantify the color of the solution.[39] This was because when AuNPs were assembled with the addition of oligomer F_a, the peak intensity at the 520 nm decreased while that at 650 nm increased. The ratio of A_{525}/A_{650} decreased when assembly of AuNPs occurred and the ratio of A_{525}/A_{650} increased when disassembly of AuNPs occurred. As shown in Fig. 2, the absorbance ratio increased first, then reached a maximum between 8 and 12 nucleotides, and finally decreased with the increase of overhang size. It is well known that the longer the overhang size in oligomer F_a, the easier it is for oligomer F_d to hybridize with the oligomer F_a.[34] This could be used to explain why the disassembly rate of AuNPs first started to increase with the length of the overhang size. However, further increasing the overhang size might result in additional steric effects. In simple terms, with the increase of overhang size, the length of oligomer F_d became longer.

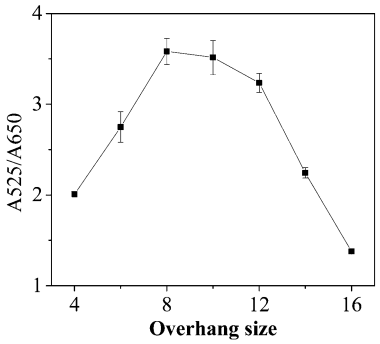

Fig. 2 The effect of overhang size on the disassembly rate of AuNPs monitored by absorption ratio of 525 nm over 650 nm.

However, the interparticle distance, which was defined by 24-mer linker DNA and a 33-nucleotide spacer, was fixed. In this regard, a longer oligomer F_d presented an additional steric effect to prevent the oligomer F_d from entering the crowded three-dimensional network. In our case, the disassembly rate of AuNPs decreased significantly if the overhang size was more than 12 nucleotides. Therefore, our findings suggested that optimization of overhang size should be considered for AuNP-based smart materials and biosensors using DNA displacement reaction.

1.3 Effect of gap size in the oligomer F_a on the disassembly rate of AuNPs. To investigate the impact of gap size on disassembly rate of AuNPs, DNA2 with a 10-nucleotide spacer and DNA1 without any spacer were used. Various numbers of gaps were introduced in oligomer F_a containing a 5 nucleotide overhang which was used in the next DNA detection experiment (see scheme in Fig. 1b). As shown in Fig. 3, the absorbance ratio of 525 nm over 650 nm started to increase with the gap size up to 8 nucleotides, reached a plateau between 8 and 16 nucleotides, and finally decreased slightly if 20 nucleotides were present in the linker DNA. This indicated that the disassembly rate increased with the increase of gap size up to 8 nucleotides. When the gap size exceeded 8 nucleotides, the gap size no longer exerted an important influence on the disassembly rate of AuNPs. Unlike the case of overhangs in oligomer F_a, here, increasing the gap size would also increase the interparticle distance, which would not pose additional steric hindrance. Nevertheless, if a large gap size was present in the oligomer F_a (*e.g.* $\geq$20), the absorbance ratio also decreased, which might be because a longer oligomer F_d could more easily form a secondary structure.[39] The longer the oligomer F_d, the higher the chance to form the secondary structure, and the smaller the chance for the oligomer F_d to hybridize with oligomer F_a to disassemble AuNPs.[39] As a result, the disassembly rate of AuNPs was inhibited here if the gap size was more than 20 nucleotides in the oligomer F_a.

1.4 Effect of spacer length on the disassembly rate of AuNPs. To investigate the effect of the spacer length on the disassembly rate of AuNPs, DNA1 with spacers of 0, 13, 23, 33 was designed, while the length of DNA2 was constant with a 10-nucleotide spacer. In the first approach, the effect of spacers on the disassembly rate of AuNPs in the presence of oligomer F_a containing a 12-overhang nucleotide (linker-O12) was studied. As shown in Fig. 4 (solid circles), the absorbance ratio of 525 nm over 650 nm increased with the length of the spacer. This phenomenon might be caused by steric hindrance in the crowded cross-linked AuNP aggregate networks. The shorter the spacer size between thiol group and hybridization sequence, the more crowded the cross-linked AuNP aggregate networks, and the more difficult it would be for oligomer F_d to enter the aggregate networks and disassemble AuNPs. Therefore, here in the presence of the oligomer F_a containing overhangs, at least 23 nucleotide spacers were needed in disassembly of AuNPs.

In the second approach, we studied the effect of spacers on the disassembly rate of AuNP aggregates in the presence of the oligomer F_a containing a 12-nucleotide gap (linker-G12). As shown in Fig. 4 (open circles), the absorbance ratio of 525 nm over 650 nm was almost constant. This suggested that the disassembly rate of AuNPs did not change as a function of spacer size. Increasing the spacer size could not change the disassembly rate.

Comparing these two approaches, Fig. 4 also showed that the absorbance ratio of disassembly of AuNP aggregates in the presence of oligomer F_a containing gaps was around two times

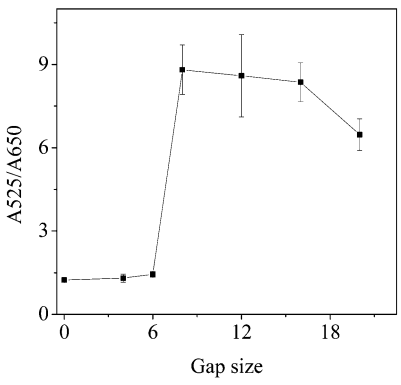

Fig. 3 The effect of gap size on the disassembly rate of AuNPs monitored by the absorption ratio of 525 nm over 650 nm.

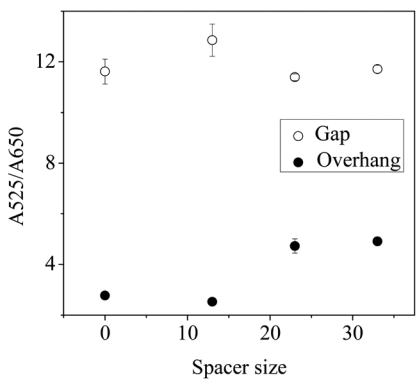

Fig. 4 The disassembly rate of AuNPs monitored by the absorbance ratio of 525 nm over 650 nm as a function of spacer size in the presence of oligomer F_a containing a 12-gap nucleotide (open circles), and that in the presence of oligomer F_a containing a 12-overhang nucleotide (solid circles).

higher than that in the presence of oligomer F_a containing overhangs. This indicated that the disassembly rate of AuNPs in the presence of oligomer F_a containing gaps was much higher than that in the presence of the oligomer F_a containing overhangs. The difference might be attributed to two possible reasons. One is that overhang sequences might result in additional steric effects which would significantly hinder the disassembly rate. In contrast, the gaps increased the interparticle distance, which relieved the steric effect. The other possible reason is that the spacer and overhang aligned on the same side which might inhibit the disassembly rate.[38]

1.5 Rapid disassembly rate of AuNPs. As mentioned previously, the disassembly rate of AuNPs could be improved remarkably when the gap size was more than 8 nucleotides in the oligomer F_a. To identify the optimal time, time-dependent monitoring of the DNA displacement reaction rate was performed. As shown in Fig. 5a, in the presence of 2 equivalents of oligomer F_d (with respect to F_a), the absorbance ratio of 525 nm over 650 nm became saturated within 50 min. It was far more rapid than the previous reports of up to 24 h.[32,36] Recently, Gang and coworkers reported the use of DNA displacement reaction to modulate the distance between adjacent AuNPs in three-dimensional superlattices within 3 h.[37] However, the DNA displacement reaction in their work could not fully restore the system to the original state. In contrast, in our work, the color of the AuNP aggregates started to turn red within 5 min, and the absorption fully restored to the original dispersed state within 50 min (see Fig. 5b, curves 1 and 3), clearly indicating the great potential for fabricating rapid colorimetric DNA biosensors.

2 Design of rapid colorimetric DNA biosensor using exonuclease III assisted signal amplification

2.1 The feasibility of the proposed sensor. Colorimetric detection of DNA based on AuNPs has attracted a lot of attention due to the merits of lower cost and fair sensitivity in comparison with fluorescent assay, and the exquisite capability of visual detection using the "naked" eye.[53–56] As a proof of the importance of the aforementioned findings, we successfully prepared a rapid colorimetric biosensor for DNA detection based on disassembly of AuNPs. In addition, to make the AuNP-based colorimetric biosensors more feasible in practical applications, we show that the signal of the AuNP-based colorimetric biosensors could be further amplified by using exonuclease III. As illustrated in Fig. 6, the sensor consists of exonuclease III, linker DNA, and two sets of thiol–DNA (DNA1 without any spacer and DNA2 with a 10-adenine spacer) which were tethered on AuNPs *via* Au–S bonds. Exonuclease III catalyzed the stepwise removal of mononucleotides from 3′-hydroxyl recessed or blunt terminus of duplex DNA. Linker DNA was divided into three segments. The first segment (colored in light blue) was the overhang in the 3′-hydroxyl terminus which performed two roles. On one hand, it prevented exonuclease III from digesting the linker DNA in the absence of target. On the other hand, it promoted hybridization of linker DNA and target. The second segment (colored in orange) was the gap which enabled target to hybridize with the linker DNA and increase the interparticle distance. The third segment (colored in red) was the hybridization sequence which was complementary with DNA1 and DNA2. Two sets of AuNPs modified with DNA1 or DNA2 were assembled with linker DNA to form AuNP aggregates. Upon addition of target and exonuclease III on the aggregates solution, target hybridized with the linker DNA to form duplex with a blunt 3′ terminus, resulting in the redispersion of AuNP aggregates. Exonuclease III catalyzed the stepwise removal of mononucleotides from this terminus, releasing the target DNA. The released target was free to hybridize with another linker DNA and underwent a new cleavage reaction, resulting in significant amplification of the signal.

Since the disassembly rate of AuNPs had an approximately linear relationship with the gap size in the presence of both target and exonuclease III (see Fig. S3 and more discussion in ESI†), a 20 gap nucleotide was used in the proposed sensor. Fig. 7 shows AuNP aggregates were not digested by exonuclease III (curves a and b), and the peak intensity was slightly increased with the addition of a low concentration of target (curve c), indicating that the target hybridized with the linker DNA. Interestingly, a remarkable increase in peak intensity was observed when the target and exonuclease III was added to the aggregates solution simultaneously (Fig. 7, curve d). This result was likely due to the cyclic hybridization with linker DNA by target DNA and subsequent cleavage of linker DNA by exonuclease III. The amplification provided by exonuclease III led to a 2.5-fold increase in the final absorbance ratio of 525 nm over 650 nm. The signal amplification provided by exonuclease III was confirmed by transmission electron microscopy. As shown in Fig. 8, the TEM image of AuNP aggregates after addition of

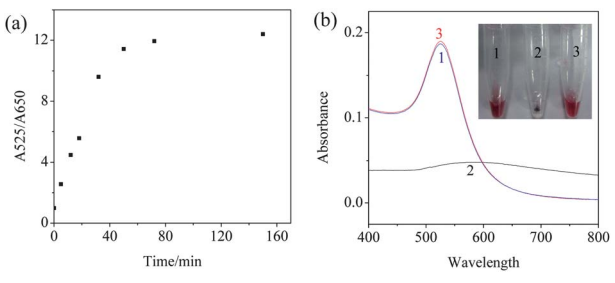

Fig. 5 (a) Time course study of disassembly of AuNPs (with a 12-nucleotide gap) monitored by the ratio of 525 nm over 650 nm. (b) Absorption spectra of dispersed DNA-AuNPs (1), AuNP aggregates (2), and redispersed AuNPs in solution after incubation for 50 min in the presence of oligomer F_d (3). The insert shows corresponding photographs.

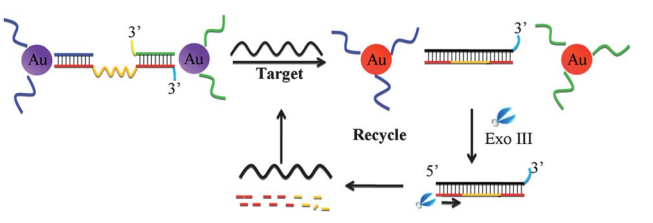

Fig. 6 Scheme of colorimetric method for DNA detection using exonuclease III assisted signal amplification and AuNP aggregates as probes.

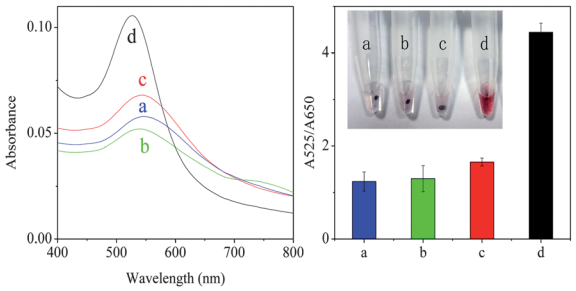

Fig. 7 UV-vis absorption spectra (left panel) and histogram (right panel) of AuNP aggregate solutions (a), AuNP aggregate solutions after addition of exonuclease III (b), gold aggregate solutions after addition of target (c), AuNP aggregate solutions after addition of target and exonuclease III (d). [Target] = 40 nM, [exonuclease III] = 60 U. All DNA sequences are listed in the ESI.†

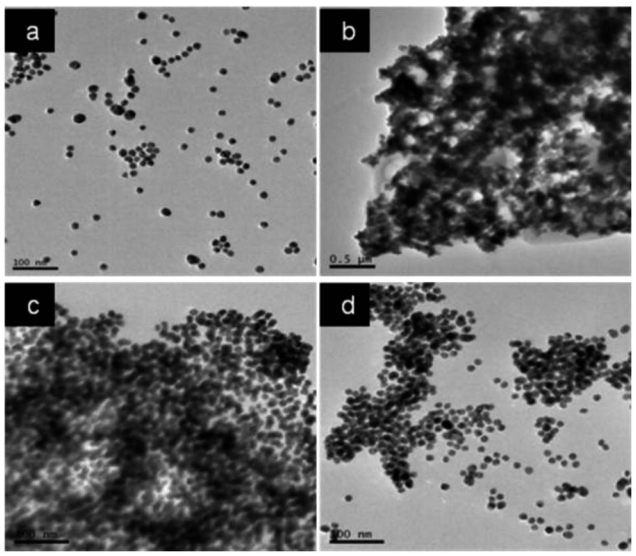

Fig. 8 TEM images of (a) mono-dispersed colloidal AuNPs, (b and c) AuNP aggregates after adding exonuclease III, and (d) AuNP aggregates after digestion by adding the target and exonuclease III. Scale bars in (a), (c) and (d) are 100 nm, and that in (b) is 500 nm. [Target] = 60 nM, [exonuclease III] = 60 U.

exonuclease III showed large aggregates, indicating that exonuclease III alone could not digest the AuNP aggregates (Fig. 8b and c). In contrast, in the presence of exonuclease III and targets, Fig. 8d showed a majority of dispersed AuNPs together with a minority of small gold AuNP aggregates, indicating that the target acted as a trigger of the exonuclease III digestion reaction.

2.2 Sensitivity of the proposed sensor. The sensitivity of the proposed colorimetric biosensor for quantitative detection of DNA was investigated using target DNAs of different concentrations. Fig. 9a showed the photographs of AuNP aggregates after addition of 60 U exonuclease III and various concentrations of target DNA. It was observed that the color of the solution turned to red gradually with the increase in the concentration of target, whereas the amounts of black precipitates decreased. Meanwhile, in UV-vis spectra, the intensity at 525 nm increased with increasing the

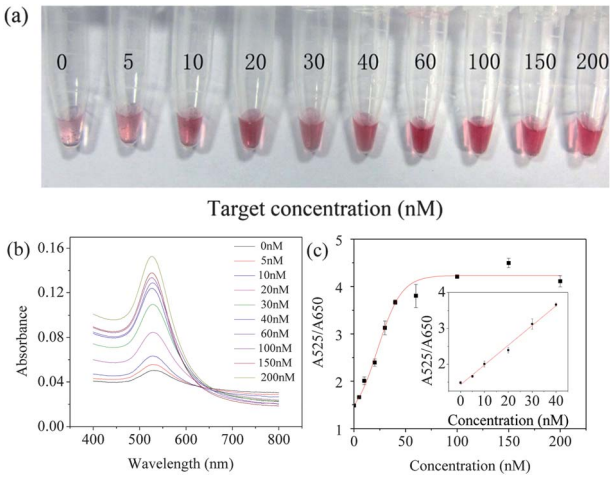

Fig. 9 (a) Photographs of AuNP aggregates after incubation with different concentrations of target DNA followed by digestion by exonuclease III, (b) corresponding UV-vis spectra, and (c) the standard curve for the relationship between the ratio of 525 nm over 650 nm and the concentration of target DNA, the inset: linear relationship between the ratio of A_{525}/A_{650} and the concentration of target DNA.

concentration of target, while that at 650 nm decreased (Fig. 9b). Fig. 9c depicts the ratio of 525 nm over 650 nm as a function of target concentration. The linear correlation was obtained in concentration from 0 nM and 40 nM and the correlation coefficient was 0.998 (inset in Fig. 9c). The detection limit of 2 nM was obtained in terms of 3 times deviation of blank sample, notably much lower than that of other colorimetric biosensors based on disassembly of AuNPs (20 nM to 50 μM).[26–31] It should be noted that the color change of the AuNP aggregate solution was observed within 5 min in this work. To decrease the detection limit of the biosensors using exonuclease III, the reaction time was compromised to 2 h, which however was still more rapid than previous reports (up to 24 h).[32] In these regards, our proposed rapid colorimetric biosensor with high sensitivity holds great potential for quantitative assay of DNA visually using the "naked" eye.

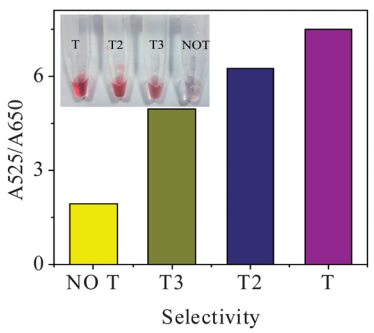

Fig. 10 Histogram of specificity of the DNA assay. No T: no target DNA was added, T: perfectly matched DNA was added; T2: two-base mismatched DNA; T3: three-base mismatched DNA. The DNA concentrations of T, T2 and T3 are 40 nM. [Linker DNA] = 100 nM. [Exonuclease III] = 60 U. Inset: the photograph of the corresponding samples. All DNA sequences are listed in the ESI.†

2.3 Selectivity of the proposed biosensor. To provide better understanding of the specificity of the experiment, perfectly matched DNA, two-base mismatched DNA and three-base mismatched DNA were chosen. The AuNP aggregates were incubated with perfectly matched DNA, two-base mismatch DNA, three-base mismatch DNA and in the absence of DNA. The histogram and corresponding photographs (Fig. 10) after addition of exonuclease III and different targets showed that as the number of mismatched bases increased, the solution turned colorless while the amount of AuNP aggregates precipitated on the bottom of Eppendorf tube increased. Further improvement of the selectivity could be achieved by increasing the spacer size and decreasing the gap size.

Conclusion

In summary, the effect of nonbase-paired regions on the disassembly rate of AuNP aggregates was investigated. First, in the presence of linker DNA containing overhang, the disassembly rate started to increase, and then reached a maximum, and finally decreased with the increase of overhang size. Secondly, in the presence of linker DNA containing gaps, the disassembly rate started to increase, and then reached a plateau, and finally decreased with the increase of gap size. Thirdly, the disassembly rate increased with the increase of the length of spacer in the presence of overhangs, while it changed little in the presence of gaps. More interestingly, we found that the disassembly rate of AuNP aggregates in the presence of gaps was much higher than that of overhangs, which might be attributed to two possible reasons. One possible reason was that the overhang sequence might result in additional steric effects which significantly inhibited the disassembly rate. The other possible reason was that the interaction between overhang and the spacer attached on AuNPs might inhibited the disassembly rate. As a result, when we introduced gaps into linker DNA, the DNA displacement reaction of AuNPs was markedly shortened to less than 50 min. As a proof of the importance of our findings, a rapid AuNP-based colorimetric DNA biosensor was successfully prepared. In addition, we showed that the signal of the biosensors could be further amplified using exonuclease III, resulting in a much lower detection limit in comparison with previous sensors similarly using AuNP aggregates as probes.

Acknowledgements

The work is supported by the National Basic Research Program of China (No. 2010CB732400), National Natural Science Foundation of China (Grant Nos. 21175021, 21205014) and the Key Program (BK2012734) from the Natural Science Foundation of Jiangsu province.

Notes and references

1 C. A. Mirkin, R. L. Letsinger, R. C. Mucic and J. J. Storhoff, *Nature*, 1996, **382**, 607–609.
2 J. Kim, C.-A. Im, Y. Jung, A. Qazi and J.-S. Shin, *Biomacromolecules*, 2010, **11**, 1705–1709.
3 S. Y. Park, A. K. Lytton-Jean, B. Lee, S. Weigand, G. C. Schatz and C. A. Mirkin, *Nature*, 2008, **451**, 553–556.
4 D. Nykypanchuk, M. M. Maye, D. van der Lelie and O. Gang, *Nature*, 2008, **451**, 549–552.
5 Y. Song, W. Wei and X. Qu, *Adv. Mater.*, 2011, **23**, 4215–4236.
6 L. Lermusiaux, A. Sereda, B. Portier, E. Larquet and S. Bidault, *ACS Nano*, 2012, **6**, 10992–10998.
7 F. A. Aldaye and H. F. Sleiman, *J. Am. Chem. Soc.*, 2007, **129**, 4130–4131.
8 T. Song and H. Liang, *J. Am. Chem. Soc.*, 2012, **134**, 10803–10806.
9 J. J. Storhoff, R. Elghanian, R. C. Mucic, C. A. Mirkin and R. L. Letsinger, *J. Am. Chem. Soc.*, 1998, **120**, 1959–1964.
10 K. Saha, S. S. Agasti, C. Kim, X. Li and V. M. Rotello, *Chem. Rev.*, 2012, **112**, 2739–2779.
11 R. Elghanian, *Science*, 1997, **277**, 1078–1081.
12 R. A. Reynolds, C. A. Mirkin and R. L. Letsinger, *J. Am. Chem. Soc.*, 2000, **122**, 3795–3796.
13 J. Liu and Y. Lu, *J. Am. Chem. Soc.*, 2003, **125**, 6642–6643.
14 W. Qu, Y. Liu, D. Liu, Z. Wang and X. Jiang, *Angew. Chem., Int. Ed.*, 2011, **50**, 3442–3445.
15 H. Xu, X. Mao, Q. Zeng, S. Wang, A.-N. Kawde and G. Liu, *Anal. Chem.*, 2009, **81**, 669–675.
16 S. Hong, I. Choi, S. Lee, Y. I. Yang, T. Kang and J. Yi, *Anal. Chem.*, 2009, **81**, 1378–1382.
17 D. X. Li, J. F. Zhang, Y. H. Jang, Y. J. Jang, D. H. Kim and J. S. Kim, *Small*, 2012, **8**, 1442–1448.
18 J. S. Lee, M. S. Han and C. A. Mirkin, *Angew. Chem., Int. Ed.*, 2007, **46**, 4093–4096.
19 X. Xue, F. Wang and X. Liu, *J. Am. Chem. Soc.*, 2008, **130**, 3244–3245.
20 J. W. Liu and Y. Lu, *Anal. Chem.*, 2004, **76**, 1627–1632.
21 S. J. Hurst, M. S. Han, A. K. R. Lytton-Jean and C. A. Mirkin, *Anal. Chem.*, 2007, **79**, 7201–7205.
22 R. C. Jin, G. S. Wu, Z. Li, C. A. Mirkin and G. C. Schatz, *J. Am. Chem. Soc.*, 2003, **125**, 1643–1654.
23 I. I. S. Lim, U. Chandrachud, L. Wang, S. Gal and C.-J. Zhong, *Anal. Chem.*, 2008, **80**, 6038–6044.
24 G. Song, C. Chen, J. Ren and X. Qu, *ACS Nano*, 2009, **3**, 1183–1189.
25 X. Xu, M. S. Han and C. A. Mirkin, *Angew. Chem., Int. Ed.*, 2007, **46**, 3468–3470.
26 L.-J. Ou, P.-Y. Jin, X. Chu, J.-H. Jiang and R.-Q. Yu, *Anal. Chem.*, 2010, **82**, 6015–6024.
27 J. Liu and Y. Lu, *J. Am. Chem. Soc.*, 2005, **127**, 12677–12683.
28 J. Liu and Y. Lu, *Adv. Mater.*, 2006, **18**, 1667–1671.
29 X. Xu, W. L. Daniel, W. Wei and C. A. Mirkin, *Small*, 2010, **6**, 623–626.
30 J. Liu and Y. Lu, *Angew. Chem., Int. Ed*, 2006, **118**, 96–100.
31 J.-S. Lee, P. A. Ulmann, M. S. Han and C. A. Mirkin, *Nano Lett.*, 2008, **8**, 529–533.
32 P. Hazarika, B. Ceyhan and C. M. Niemeyer, *Angew. Chem., Int. Ed.*, 2004, **43**, 6469–6471.
33 Z. Zhang, Q. Cheng and P. Feng, *Angew. Chem., Int. Ed.*, 2009, **48**, 118–122.
34 Q. Q. Li, G. Y. Luan, Q. P. Guo and J. X. Liang, *Nucleic Acids Res.*, 2002, **30**, e5.

35 J. P. Cheng, Y. Y. Zhang and Q. G. Li, *Nucleic Acids Res.*, 2004, **32**, e61.
36 C. K. Tison and V. T. Milam, *Langmuir*, 2007, **23**, 9728–9736.
37 M. M. Maye, M. T. Kumara, D. Nykypanchuk, W. B. Sherman and O. Gang, *Nat. Nanotechnol.*, 2010, **5**, 116–120.
38 J. Liu and Y. Lu, *J. Am. Chem. Soc.*, 2007, **129**, 8634–8643.
39 B. D. Smith, N. Dave, P.-J. J. Huang and J. Liu, *J. Phys. Chem. C*, 2011, **115**, 7851–7857.
40 X. Zuo, F. Xia, Y. Xiao and K. W. Plaxco, *J. Am. Chem. Soc.*, 2010, **132**, 1816–1818.
41 M. Zhang, Y. M. Guan and B. C. Ye, *Chem. Commun.*, 2011, **47**, 3478–3480.
42 R. Freeman, X. Liu and I. Willner, *Nano Lett.*, 2011, **11**, 4456–4461.
43 C. Zhao, L. Wu, J. Ren and X. Qu, *Chem. Commun.*, 2011, **47**, 5461–5463.
44 F. Xuan, X. Luo and I. M. Hsing, *Anal. Chem.*, 2012, **84**, 5216–5220.
45 J. J. Li, Y. Chu, B. Y. Lee and X. S. Xie, *Nucleic Acids Res.*, 2008, **36**, e36.
46 W. Xu, X. Xue, T. Li, H. Zeng and X. Liu, *Angew. Chem., Int. Ed.*, 2009, **48**, 6849–6852.
47 Y. V. Gerasimova, S. Peck and D. M. Kolpashchikov, *Chem. Commun.*, 2010, **46**, 8761.
48 H. D. Hill and C. A. Mirkin, *Nat. Protoc.*, 2006, **1**, 324–336.
49 J. Liu and Y. Lu, *Nat. Protoc.*, 2006, **1**, 246–252.
50 S. J. Hurst, A. K. R. Lytton-Jean and C. A. Mirkin, *Anal. Chem.*, 2006, **78**, 8313–8318.
51 K. E. Sapsford, D. Park, E. R. Goldman, E. E. Foos, S. A. Trammell, D. A. Lowy and M. G. Ancona, *Langmuir*, 2008, **24**, 10245–10252.
52 J. Zhang, S. Song, L. Wang, D. Pan and C. Fan, *Nat. Protoc.*, 2007, **2**, 2888–2895.
53 Y. Zhang, J. Hu and C. Y. Zhang, *Anal. Chem.*, 2012, **84**, 9544–9549.
54 W. Shen, H. Deng and Z. Gao, *J. Am. Chem. Soc.*, 2012, **134**, 14678–14681.
55 H. Li and L. Rothberg, *Proc. Natl. Acad. Sci. U. S. A.*, 2004, **101**, 14036–14039.
56 L. Cui, G. Ke, W. Y. Zhang and C. J. Yang, *Biosens. Bioelectron.*, 2011, **26**, 2796–2800.

